

A Large Area Organic Solar Module with Non-Halogen Solvent Treatment, High Efficiency, and Decent Stability

Shuchao Zhang, Hongbin Chen, Peiran Wang, Shitong Li, Zhixiang Li, Yuzhong Huang, Jian Liu, Zhaoyang Yao, Chenxi Li, Xiangjian Wan,* and Yongsheng Chen*

It is a challenge to fabricate organic solar modules with the combination of high efficiency, good stability, and green solvent treatment. To address the issue, active layer materials still play crucial roles. Herein, a non-fullerene acceptor CH7 with the extended conjugation central unit and long-branched side chains is reported for the fabrication of high-performance large-area modules. The long-branched alkyl chains can ensure CH7 to have good solubility in non-halogen solvent *o*-xylene (OX). Meanwhile, the steric hindrance of long-branched alkyl chains can suppress molecular excessive aggregation. The inverted structure prototype device based on PM6:CH7 and processed with OX showed a promising power conversion efficiency (PCE) of 17.49% mainly due to the favorable active layer morphology. Based on the small area device results, processed from OX, a 25.2 cm² module is fabricated and demonstrates a high PCE of 14.42% and good photo stability with maintaining 93% of its initial efficiency after 500 h continuous illumination. Moreover, the module also shows decent thermal stability, maintaining with 82% of its original efficiency after the thermal stress at 65 °C for 500 h.

been paid to large-area OSC modules.^[9–13] Especially, the boosting efficiencies of NFA-based OSCs have provided more opportunities for high-efficiency large-area modules and many promising results have been reported.^[13–28] Some recent representative modules are summarized in Table S1, Supporting Information.

Despite the impressive progress on efficiencies, there are still some concerns needed to be seriously addressed for organic solar modules. One important concern is stability. Although PCEs of OSCs have rapidly increased in the past years, stability issues have received less attention, especially on modules.^[29,30] Although some OSCs with promising stabilities have been reported,^[31–33] only a few small area devices show the combination of high efficiencies and good stabilities.^[34–38] Another concern is the toxicity of solution-processed solvents.

Halogen solvents such as chlorobenzene and chloroform are currently the dominant solvents used for fabricating small-area devices and large-area modules. However, the toxicity and threat of halogen solvents to human health and the environment will be not acceptable for future large-scale manufacture of OSC modules.^[39] Consequently, non-halogen solvent (eco-friendly solvent) processed OSCs have received increasing attention. Many strategies, e.g., modifying the active layer material structures,^[15] additives,^[40] ternary active layer,^[14] have been proposed to fabricate devices using non-halogen solvents. However, the efficiencies of non-halogen solvent processed devices still fall behind those processed from halogen solvents mainly due to the unfavorable active layer morphologies. To date, only several prototype devices processed with non-halogen solvents were reported with efficiencies of over 17%.^[14,41–46] To our knowledge, only two cases with efficiencies over 14% were achieved for non-halogen solvent-processed modules.^[14,15]

From the perspective of the application, it is necessary for a module that simultaneously shows high efficiency, good stability, and green solvents treatment. It is an attractive target but a challenge for module fabrication, which requires strategies and efforts from multiple perspectives, e.g., active layer design, morphology control, interface layer engineering, module structure, process strategies, etc. Among them, active layer materials always play critical roles in the preparation of high-performance modules. To date, most state-of-the-art modules are fabricated

1. Introduction

In the past decade, organic solar cells (OSCs) have made remarkable progress and achieved power conversion efficiencies (PCEs) exceeding 19% mainly owing to the rapid development of active layer materials, especially non-fullerene acceptors (NFAs) and device engineering.^[1–8] However, most studies in the OSC community have focused on devices processed via spin coating with areas below 0.1 cm². With the continuous improvements in the performance of OSCs, lab-to-manufacturing translation is necessary for future applications. In recent years, much attention has

S. Zhang, H. Chen, P. Wang, S. Li, Z. Li, Y. Huang, J. Liu, Z. Yao, C. Li, X. Wan, Y. Chen

State Key Laboratory of Elemento-Organic Chemistry
The Centre of Nanoscale Science and Technology and Key Laboratory of Functional Polymer Materials
College of Chemistry

Haihe Laboratory of Sustainable Chemical Transformations
Renewable Energy Conversion and Storage Center (RECAST)
Nankai University
Tianjin 300071, China
E-mail: xjwan@nankai.edu.cn; yschen99@nankai.edu.cn

 The ORCID identification number(s) for the author(s) of this article can be found under <https://doi.org/10.1002/solr.202300029>.

DOI: 10.1002/solr.202300029

based on Y6 and its derivatives due to the high efficiencies of their prototype devices. But, little attention is paid to stability and green solvent treatment at the same time.

Recently, our group reported a series of acceptors with extended conjugation central cores and achieved PCEs over 18% for prototype devices with normal device structures.^[47,48] In this work, to fabricate modules with high efficiency, good stability, and non-halogen solvents treatment, we design an acceptor CH7 long-branched alkyl chains on the dithienothiophen[3.2-b]-pyrrolobenzothiadiazole central unit. The design of this molecule is based on the following three considerations. Firstly, high efficiency is expected for CH7-based devices since CH7 has the same molecular skeleton and only different lengths of alkyl chains compared with its parent molecules which showed PCEs over 18%.^[47,48] Second, the long-branched alkyl chains can enhance the solubility of CH7 and ensure it is processed in non-halogen solvents. Third, the steric hindrance of long-branched alkyl chains can suppress molecular excessive aggregation and might be suitable for the fabrication of devices with an inverted structure that has higher stability than those of normal structure.^[49]

As expected, the prototype inverted structure device based on PM6:CH7 and processed with a non-halogen solvent o-xylene (OX) showed a PCE of 17.49% after device optimization. Based on the small-area device results, a large-area module with an active layer area of 25.2 cm² was fabricated with non-halogen solvent OX. The module demonstrated a high PCE of 14.42% and good photostability with maintaining 93% of its initial efficiency after 500 h of continuous illumination. Moreover, the module also showed decent thermal stability, maintaining 82% of its original efficiency after the thermal stress at 65 °C for 500 h. Overall,

this work demonstrates a promising module case with high efficiency, decent stability, and eco-friendly solvent treatment.

2. Results and Discussion

The chemical structure of CH7 is shown in **Figure 1a**. It was synthesized following the method we have reported previously,^[47] and the detailed synthesis procedure is provided in Supporting Information. As shown in **Figure 1b**, CH7 shows a maximum absorption (λ_{max}) peak located at 730 nm in chloroform (CF) solution. Compared with its solution absorption in CF, CH7 solid film absorption processed from CF solution is red-shifted by 70 nm with λ_{max} at 800 nm. While the absorption peak of CH7 in OX solution is located at 710 nm, which is slightly blue-shifted compared with that in CF solution. But, the absorption peak of the film processed from OX is at 799 nm, which is nearly the same as that of CF, implying the similar aggregation behavior of CH7 in the films cast from CF and OX solution. The energy levels of CH7 were investigated by cyclic voltammetry (CV). From the onset reduction and oxidation potentials of the CV curves, the lowest unoccupied molecular orbital (LUMO) and the highest occupied molecular orbital (HOMO) levels of CH7 were estimated to be -3.75 and -5.74 eV, respectively, which is well matched with donor polymer PM6 (**Figure 1c**).

OSCs with the inverted structure of ITO/ZnO/NMA/PM6:CH7/MoO₃/Ag (**Figure 1d**) were fabricated to evaluate the photovoltaic performance of CH7. Herein, PM6 is selected as a donor owing to its matched energy levels and complementary absorption with CH7. NMA is a modification layer on ZnO that we have reported recently.^[36] Detailed device fabrication and

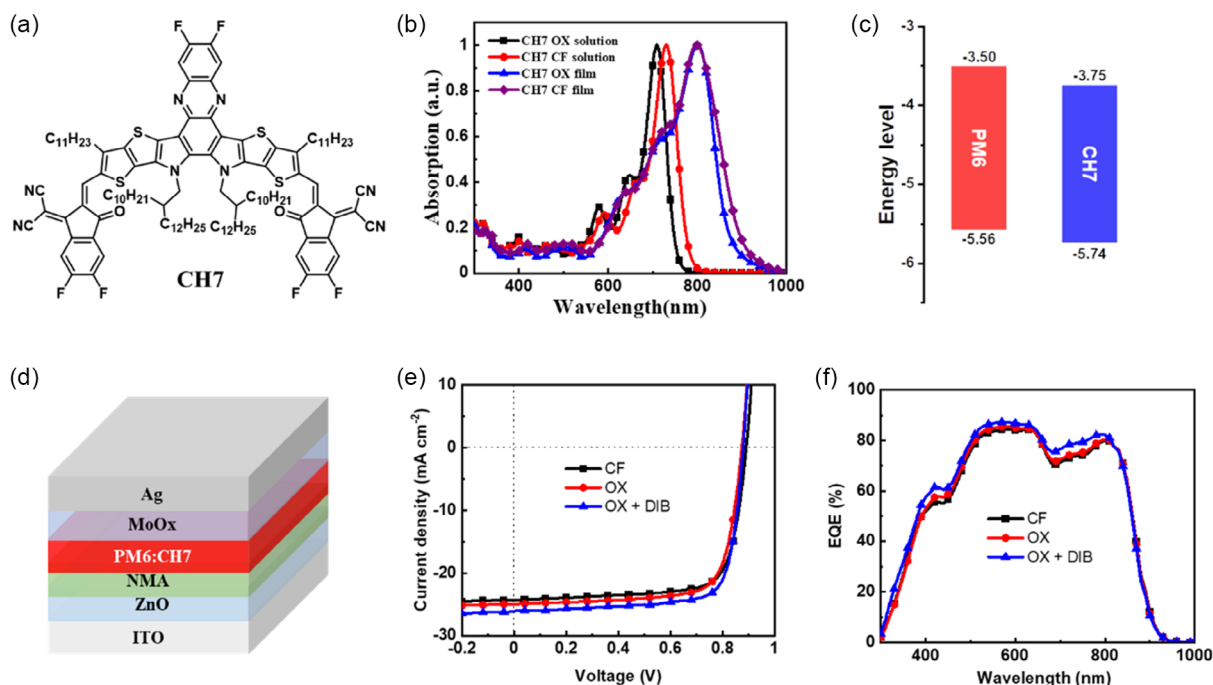


Figure 1. a) Chemical structure of CH7. b) Absorption spectra of CH7 in solutions and as thin films. c) Energy level diagram of PM6 and CH7. d) Device architecture of PM6:CH7-based organic solar cells (OSCs). e) J–V and f) external quantum efficiency (EQE) curves for devices processed with CF, OX, and OX + DIB.

optimization conditions are provided in Supporting Information. First, the devices processed by CF and OX were fabricated and compared to check the influence of the two solvents on the device performances. The device processed from CF showed a PCE of 16.27% with a V_{oc} of 0.890 V, a J_{sc} of 24.31 mA cm⁻², and a FF of 75.19%. In contrast, the OX-processed device demonstrated a slightly higher PCE of 16.44%, which is ascribed to the enhanced current due to the fine morphology of the active layer processed from OX as will be discussed below. Thus, OX was used as a solvent to further optimize device performances. With 1,4-diiodobenzene (DIB) as an additive, the optimized device of PM6:CH7 cast from OX solvent showed a PCE of 17.49% with an improved J_{sc} and FF compared with the control device. The current density–voltage (J - V) curves of devices cast from CF, OX, and OX with DIB (OX + DIB) are illustrated in Figure 1e, and their corresponding photovoltaic parameters are summarized in Table 1. As shown in Figure 1f, the external quantum efficiency (EQE) curve of the device cast from OX with DIB demonstrated higher photon response compared with the other two devices. The integrated J_{sc} from EQE curves is in good agreement with the J_{sc} from the J - V curves.

To understand the difference in the photovoltaic device performances, the properties of the charge transport, exciton dissociation, and charge generation of the three devices cast from CF, OX, and OX with DIB were investigated and compared. The space-charge-limited current (SCLC) method was employed to measure the charge mobilities of the blend films. As shown in Figure 2a, the electron/hole mobilities of the blend films cast

Table 1. Photovoltaic parameters of OSCs under AM 1.5G, 100 mW cm⁻².

Solvent	V_{oc} [V]	J_{sc} [mA cm ⁻²]	$J_{cal.}$ [mA cm ⁻²]	FF [%]	PCE [%]
CF	0.890	24.31	23.72	75.19	16.27
OX	0.884	24.95	23.98	74.97	16.44
OX + DIB	0.881	25.82	24.68	76.88	17.49

from CF and OX showed similar values of 1.50/2.26 and 1.56/2.31, respectively. But, the blend film cast from OX with DIB yielded many improved mobilities with electron/hole values of 1.96/2.60, which is due to the intense donor and acceptor packing as discussed below. The increased and balanced mobilities contributed to the improved performance of the device cast from OX with DIB. The dependence of photocurrent density (J_{ph}) versus effective voltage (V_{eff}) was measured to investigate the exciton dissociation and charge generation properties. The exciton dissociation probability (P_{diss}), calculated from J_{ph} under the short-circuit condition divided by the saturated photocurrent density (J_{sat}), were 95.57%, 95.91%, and 97.10% for the devices cast from CF, OX, and OX with DIB, respectively. The results demonstrate that the device casting from OX with DIB showed higher efficient exciton dissociation compared with the other two devices. To study the behavior of charge recombination of the three devices, the dependence of the J - V characteristics on light intensity (P_{light}) was measured. The plots of light-intensity dependence (P) of J_{sc} ($J_{sc} \propto P^\alpha$), where the exponent of α being close to

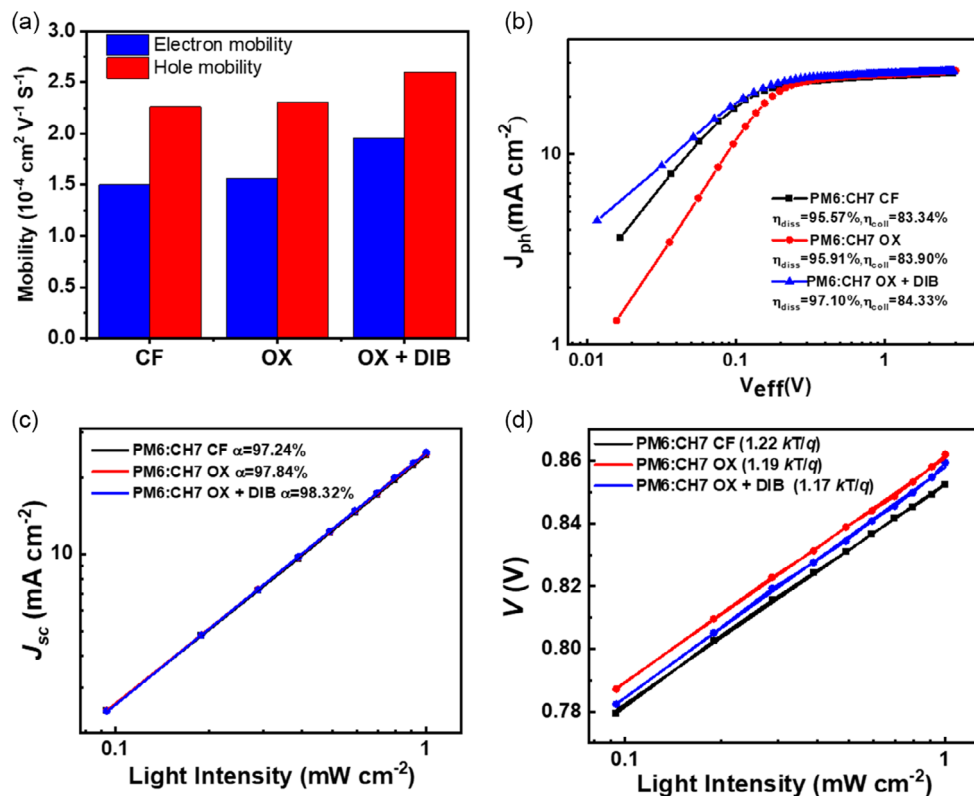


Figure 2. a) Charge-carrier mobility histogram, b) J_{ph} - V_{eff} curves, c) dependence of J_{sc} , and d) V_{oc} on the light intensity of the devices process with CF, OX, and OX + DIB.

1 reflects a weak bimolecular recombination, were measured and displayed in Figure 2c. The J_{sc} of the three devices was almost linearly correlated with P , with the α values 0.972, 0.978, and 0.983 for the devices cast from CF, OX, and OX with DIB, respectively, indicating the less bimolecular recombination in the three devices, especially the device cast from OX with DIB. When the slope of V_{oc} versus the $\ln(P_{light})$ is equal to $1kT/q$, where k is the Boltzmann constant, T is the temperature in Kelvin, and q is the elementary charge, the dominant recombination mechanism is bimolecular recombination. Trap-assisted recombination is dominant when the slope of V_{oc} versus the $\ln(P_{light})$ is $2kT/q$. As shown in Figure 2d, the slopes of V_{oc} versus the $\ln(P_{light})$ are $1.22kT/q$ and $1.19kT/q$, and $1.17kT/q$ for the devices cast from CF, OX, and OX with DIB, respectively. The small slopes implied the low trap density and weak trap-assistant recombination in the three devices, especially the device cast from OX with DIB.

The morphologies of the three devices were characterized by atomic force microscopy (AFM) and transmission electron microscopy (TEM). As illustrated in Figure 3, the three blend

films all showed smooth surface morphologies with fibrillar networks. The root-mean-square roughness (R_q) values are 1.27, 1.34, and 1.16 nm for the blend films cast from CF, OX, and OX with DIB, respectively. The statistical fiber size in the three blending films is around 29.7, 26.1, and 21.4 nm, respectively, which are consistent with TEM results as shown in Figure 3g–i. There are clearly larger fiber structures in the blending film cast from CF (Figure 3g) than the other two blending films. The blending film casted from OX with DIB depicted a smooth fiber network without clear large aggregation. The grazing incidence wide-angle X-ray scattering (GIWAXS) was used to investigate the molecular stacking and orientation of CH7 and its blend films cast under different conditions. As shown in Figure S4, Supporting Information, the neat films of CH7 cast from CF and OX both show an obvious π – π stacking diffraction peak (010) at around 1.60 \AA^{-1} with a d spacing of 3.9 \AA in the out-of-plane (OOP) direction, indicating a face-on orientation. The blend films of PM6:CH7 cast from CF, OX, and OX with DIB all exhibit the face-on orientations with clear π – π stacking diffraction peaks (010) in the OOP directions. As listed in Table S11, Supporting Information, the blending film

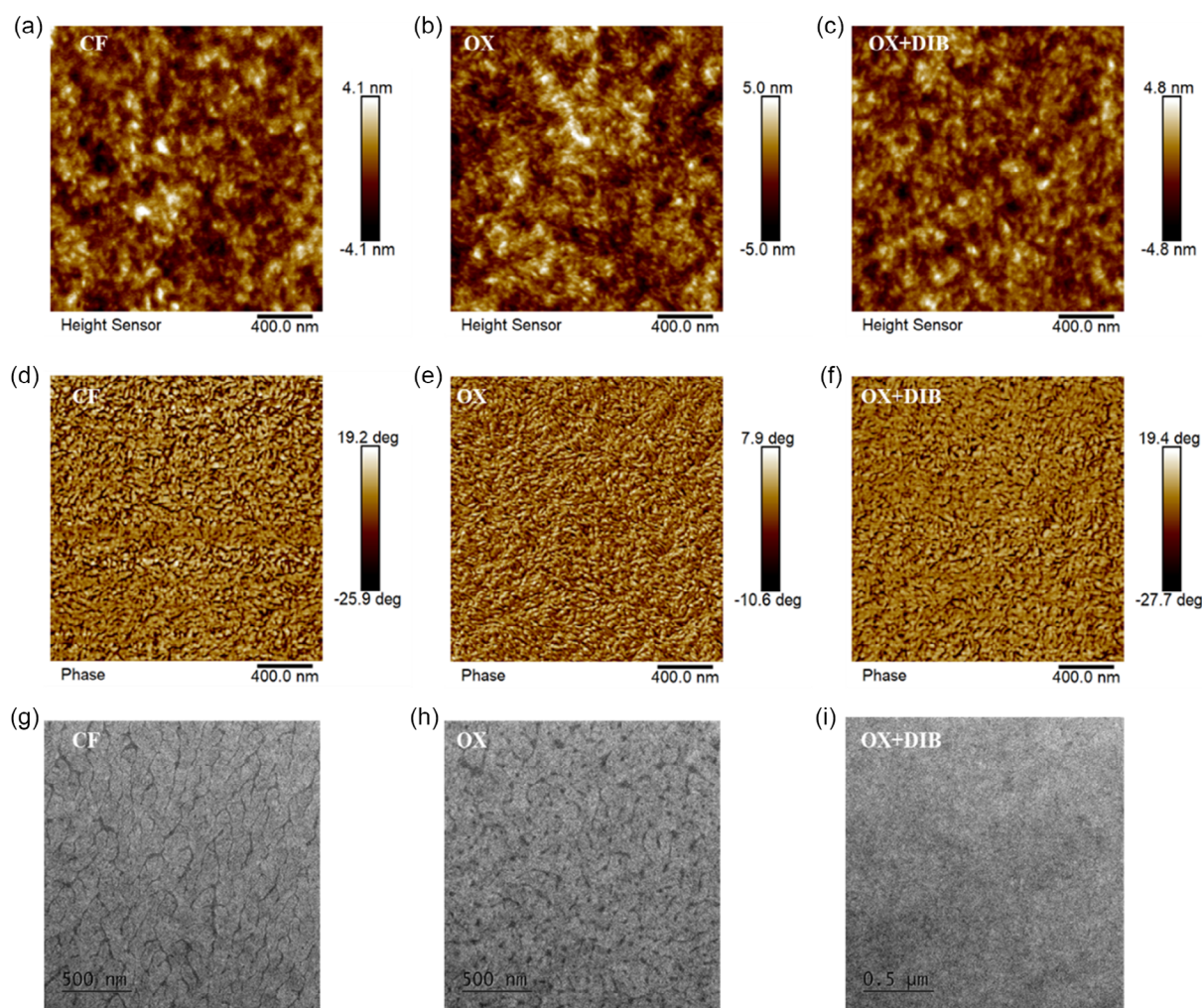


Figure 3. a–c) Atomic force microscopy (AFM) height and d–f) phase images, and g–i) transmission electron microscope (TEM) images of active layer processed from CF, OX, and OX + DIB.

cased from OX with DIB has a slightly larger crystal coherence length (CCL) of 20.1 Å in the (010) OOP direction, which indicates a relatively stronger crystallinity and is consistent with its enhanced mobilities as discussed above.

We fabricated a module consisting of seven subcells connected in series (Figure S5, Supporting Information) using OX as the active layer processing solvent with DIB as an additive. A photo of the module with an active area of 25.2 cm² is depicted in **Figure 4a**. As shown in Figure 4b, the module exhibits an outstanding PCE of 14.42%, with a V_{oc} of 6.01 V, a J_{sc} of 3.42 mA cm⁻², and a FF of 70.17%, which is the highest efficiency for OSC modules fabricated with non-halogen solvents and with an active area exceeding 20 cm² (Table S1, Supporting Information). The photostability of the module was tested under 1 sun illumination simulated white LED with max power point (MPP) tracking in the N₂-filled glove box with a temperature around 25 °C. As shown in Figure 4c, the module showed good photostability, remaining 93% of its initial efficiency after 500 h continuing illumination. Moreover, the module also showed decent thermal stability, maintaining 82% of its original efficiency after the thermal stress at 65 °C for 500 h. The performance of the module is among the best results for organic modules simultaneously with high efficiency and decent stability (Table S1, Supporting Information). The photocatalysis of ZnO in inverted structure devices is one of the main factors that leads to the deterioration of photostability.^[31] In our case, NMA was used as the modified layer on ZnO to form a hybrid electron transport layer, which could reduce the content of defective oxygen on the surface of ZnO film and suppress ZnO's capacity for photocatalysis as we reported previously.^[36] Therefore, the module showed good photostability. Compared with the good photostability, the relatively low thermal stability of the module might come from the less densely packing of acceptor

CH7 with the large and long branched aliphatic side chains.^[46] In contrast, in view of the promising application for semitransparent OSCs as power-generating windows in building-integrated photovoltaics, green-house, etc.,^[26,50] we fabricated a semitransparent module based on the above active layer with an ultrathin transparent Ag electrode and MoO₃ anti-reflective layer (Figure 4e). After optimization, the semitransparent module exhibits a PCE of 9.69% with an average visible transmittance (AVT) 27.5% (Figure 4f).

3. Conclusion

In summary, we have designed an acceptor CH7 with the extended conjugation central core and long-branched side chains. Based on PM6:CH7, the prototype small area OSCs with the inverted structure were fabricated and showed a high PCE of 17.49%, which is mainly attributed to the high and balanced mobilities and reasonable morphology. Based on the above small-area device of PM6:CH7, a large-area module with an active layer of 25.2 cm² was fabricated using the non-halogen solvent OX. The module exhibited an outstanding PCE of 14.42% and demonstrated a promising photo-stability, maintaining 93% initial efficiency after light aging for 500 h. This work has provided a promising case for organic solar modules with the combination of high efficiency, good stability, and green solvent treatment. It is also believed that higher performance organic solar modules can be manufactured via the delicate design of active layer materials and careful device optimizations.

Supporting Information

Supporting Information is available from the Wiley Online Library or from the author.

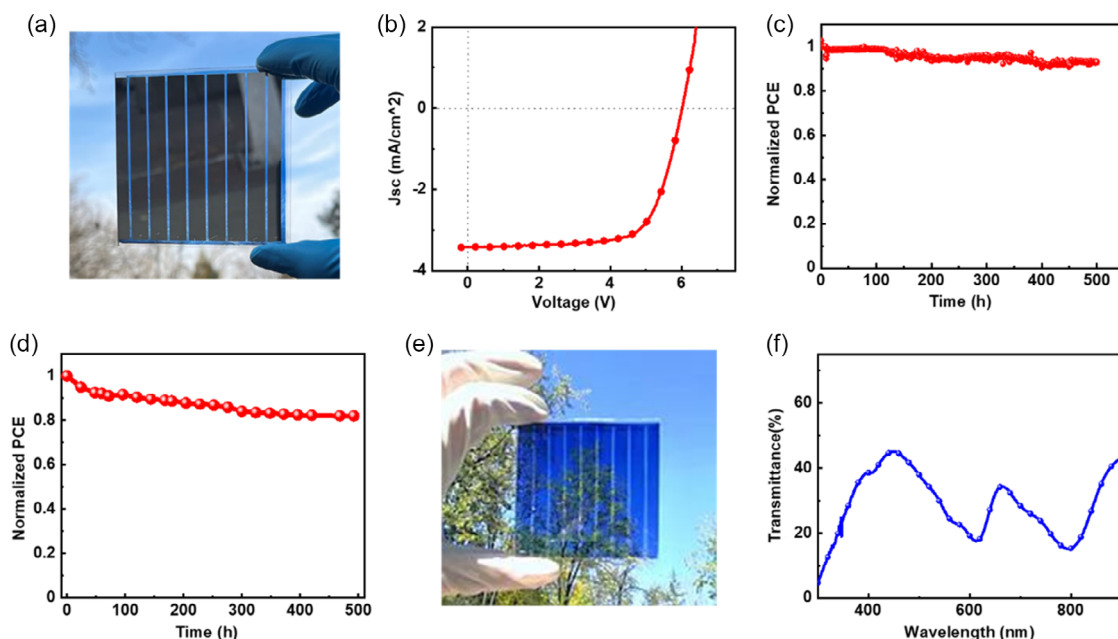


Figure 4. a) Images of the opaque module based on PM6:CH7 with an active area of 25.2 cm². b) J - V curve of the opaque module. c) MPP stability test of the opaque module under MPP tracking with continuous illumination of 100 mW cm⁻² LED arrays. d) Thermal stability of the above opaque module at 65 °C. e) Image of the semitransparent module based on PM6:CH7. f) Transmittance spectrum of the above semi-transparent module.

Acknowledgements

The author gratefully acknowledges the financial support from NSFC (52025033 and 21935007) MoST (2022YFB4200400, 2019YFA0705900) of China, Tianjin city (20JCZDJC00740), 111 Project (B12015), and the Haihe Laboratory of Sustainable Chemical Transformations.

Conflict of Interest

The authors declare no conflict of interest.

Data Availability Statement

The data that support the findings of this study are available in the supplementary material of this article.

Keywords

efficiency, modules, non-halogen solvents, organic solar cells, stability

Received: January 15, 2023

Revised: January 24, 2023

Published online: February 3, 2023

- [1] Y. Cui, Y. Xu, H. Yao, P. Bi, L. Hong, J. Zhang, Y. Zu, T. Zhang, J. Qin, J. Ren, Z. Chen, C. He, X. Hao, Z. Wei, J. Hou, *Adv. Mater.* **2021**, *33*, e2102420.
- [2] C. He, Y. Pan, Y. Ouyang, Q. Shen, Y. Gao, K. Yan, J. Fang, Y. Chen, C.-Q. Ma, J. Min, C. Zhang, L. Zuo, H. Chen, *Energy Environ. Sci.* **2022**, *15*, 2537.
- [3] L. Meng, Y. Zhang, X. Wan, C. Li, X. Zhang, Y. Wang, X. Ke, Z. Xiao, L. Ding, R. Xia, H.-L. Yip, Y. Cao, Y. Chen, *Science* **2018**, *361*, 1094.
- [4] R. Sun, Y. Wu, X. Yang, Y. Gao, Z. Chen, K. Li, J. Qiao, T. Wang, J. Guo, C. Liu, X. Hao, H. Zhu, J. Min, *Adv. Mater.* **2022**, *34*, e2110147.
- [5] X. Wan, C. Li, M. Zhang, Y. Chen, *Chem. Soc. Rev.* **2020**, *49*, 2828.
- [6] Y. Wei, Z. Chen, G. Lu, N. Yu, C. Li, J. Gao, X. Gu, X. Hao, G. Lu, Z. Tang, J. Zhang, Z. Wei, X. Zhang, H. Huang, *Adv. Mater.* **2022**, *34*, e2204718.
- [7] G. Zhang, F. R. Lin, F. Qi, T. Heumuller, A. Distler, H. J. Egelhaaf, N. Li, P. C. Y. Chow, C. J. Brabec, A. K. Jen, H. L. Yip, *Chem. Rev.* **2022**, *122*, 14180.
- [8] L. Zhu, M. Zhang, J. Xu, C. Li, J. Yan, G. Zhou, W. Zhong, T. Hao, J. Song, X. Xue, Z. Zhou, R. Zeng, H. Zhu, C. C. Chen, R. C. I. MacKenzie, Y. Zou, J. Nelson, Y. Zhang, Y. Sun, F. Liu, *Nat. Mater.* **2022**, *21*, 656.
- [9] G. A. D. R. Benatto, B. Roth, M. Corazza, R. R. Sondergaard, S. A. Gevorgyan, M. Jorgensen, F. C. Krebs, *Nanoscale* **2016**, *8*, 318.
- [10] Y. W. Han, S. J. Jeon, H. S. Lee, H. Park, K. S. Kim, H.-W. Lee, D. K. Moon, *Adv. Energy Mater.* **2019**, *9*, 1902065.
- [11] X. Meng, L. Zhang, Y. Xie, X. Hu, Z. Xing, Z. Huang, C. Liu, L. Tan, W. Zhou, Y. Sun, W. Ma, Y. Chen, *Adv. Mater.* **2019**, *31*, 1903649.
- [12] G. Wang, J. Zhang, C. Yang, Y. Wang, Y. Xing, M. A. Adil, Y. Yang, L. Tian, M. Su, W. Shang, K. Lu, Z. Shuai, Z. Wei, *Adv. Mater.* **2020**, *32*, 2005153.
- [13] A. Distler, C. J. Brabec, H. J. Egelhaaf, *Prog. Photovoltaics Res. Appl.* **2021**, *29*, 24.
- [14] H. Chen, R. Zhang, X. Chen, G. Zeng, L. Kobera, S. Abbrent, B. Zhang, W. Chen, G. Xu, J. Oh, S.-H. Kang, S. Chen, C. Yang, J. Brus, J. Hou, F. Gao, Y. Li, Y. Li, *Nat. Energy* **2021**, *6*, 1045.
- [15] S. Dong, T. Jia, K. Zhang, J. Jing, F. Huang, *Joule* **2020**, *4*, 2004.
- [16] X. Dong, Y. Jiang, L. Sun, F. Qin, X. Zhou, X. Lu, W. Wang, Y. Zhou, *Adv. Funct. Mater.* **2022**, *32*, 2110209.
- [17] J. Y. Fan, Z. X. Liu, J. Rao, K. Yan, Z. Chen, Y. Ran, B. Yan, J. Yao, G. Lu, H. Zhu, C. Z. Li, H. Chen, *Adv. Mater.* **2022**, *34*, e2110569.
- [18] E. Feng, Y. Han, J. Chang, H. Li, K. Huang, L. Zhang, Q. Luo, J. Zhang, C. Ma, Y. Zou, L. Ding, J. Yang, *J. Semicond.* **2022**, *43*, 100501.
- [19] Y. W. Han, H. S. Lee, D. K. Moon, *ACS Appl. Mater. Interfaces* **2021**, *13*, 19085.
- [20] K.-M. Huang, C.-M. Lin, S.-H. Chen, C.-S. Li, C.-H. Hu, Y. Zhang, H.-F. Meng, C.-Y. Chang, Y.-C. Chao, H.-W. Zan, L. Huo, P. Yu, *Sol. RRL* **2019**, *3*, 1900071.
- [21] S. Jeong, B. Park, S. Hong, S. Kim, J. Kim, S. Kwon, J. H. Lee, M. S. Lee, J. C. Park, H. Kang, K. Lee, *ACS Appl. Mater. Interfaces* **2020**, *12*, 41877.
- [22] Z. Jia, Z. Chen, X. Chen, J. Yao, B. Yan, R. Sheng, H. Zhu, Y. Yang, *Photonics Res.* **2021**, *9*, 324.
- [23] C.-Y. Liao, Y. Chen, C.-C. Lee, G. Wang, N.-W. Teng, C.-H. Lee, W.-L. Li, Y.-K. Chen, C.-H. Li, H.-L. Ho, P. H.-S. Tan, B. Wang, Y.-C. Huang, R. M. Young, M. R. Wasielewski, T. J. Marks, Y.-M. Chang, A. Facchetti, *Joule* **2020**, *4*, 189.
- [24] C.-Y. Liao, Y.-T. Hsiao, K.-W. Tsai, N.-W. Teng, W.-L. Li, J.-L. Wu, J.-C. Kao, C.-C. Lee, C.-M. Yang, H.-S. Tan, K.-H. Chung, Y.-M. Chang, *Sol. RRL* **2021**, *5*, 2000749.
- [25] R. Sun, Q. Wu, J. Guo, T. Wang, Y. Wu, B. Qiu, Z. Luo, W. Yang, Z. Hu, J. Guo, M. Shi, C. Yang, F. Huang, Y. Li, J. Min, *Joule* **2020**, *4*, 407.
- [26] D. Wang, Y. Li, G. Zhou, E. Gu, R. Xia, B. Yan, J. Yao, H. Zhu, X. Lu, H.-L. Yip, H. Chen, C.-Z. Li, *Energy Environ. Sci.* **2022**, *15*, 2629.
- [27] L. Zhan, S. Yin, Y. Li, S. Li, T. Chen, R. Sun, J. Min, G. Zhou, H. Zhu, Y. Chen, J. Fang, C. Q. Ma, X. Xia, X. Lu, H. Qiu, W. Fu, H. Chen, *Adv. Mater.* **2022**, *34*, e2206269.
- [28] B. Zhang, F. Yang, S. Chen, H. Chen, G. Zeng, Y. Shen, Y. Li, Y. Li, *Adv. Funct. Mater.* **2022**, *32*, 2202011.
- [29] Q. Burlingame, M. Ball, Y.-L. Loo, *Nat. Energy* **2020**, *5*, 947.
- [30] L. Duan, A. Uddin, *Adv. Sci.* **2020**, *7*, 1903259.
- [31] Y. Li, X. Huang, K. Ding, H. K. M. Sheriff, Jr., L. Ye, H. Liu, C. Z. Li, H. Ade, S. R. Forrester, *Nat. Commun.* **2021**, *12*, 5419.
- [32] Q. Burlingame, X. Huang, X. Liu, C. Jeong, C. Coburn, S. R. Forrester, *Nature* **2019**, *573*, 394.
- [33] X. Xu, J. Xiao, G. Zhang, L. Wei, X. Jiao, H.-L. Yip, Y. Cao, *Sci. Bull.* **2020**, *65*, 208.
- [34] Y. Liang, D. Zhang, Z. Wu, T. Jia, L. Luer, H. Tang, L. Hong, J. Zhang, K. Zhang, C. J. Brabec, N. Li, F. Huang, *Nat. Energy* **2022**, *7*, 1180.
- [35] R. Sun, W. Wang, H. Yu, Z. Chen, X. Xia, H. Shen, J. Guo, M. Shi, Y. Zheng, Y. Wu, W. Yang, T. Wang, Q. Wu, Y. Yang, X. Lu, J. Xia, C. J. Brabec, H. Yan, Y. Li, J. Min, *Joule* **2021**, *5*, 1548.
- [36] S. Li, Q. Fu, L. Meng, X. Wan, L. Ding, G. Lu, G. Lu, Z. Yao, C. Li, Y. Chen, *Angew. Chem., Int. Ed.* **2022**, *61*, e202207397.
- [37] Q. Liao, Q. Kang, Y. Yang, Z. Zheng, J. Qin, B. Xu, J. Hou, *CCS Chem.* **2022**, *4*, 938.
- [38] Y. Han, H. Dong, W. Pan, B. Liu, X. Chen, R. Huang, Z. Li, F. Li, Q. Luo, J. Zhang, Z. Wei, C. Q. Ma, *ACS Appl. Mater. Interfaces* **2021**, *13*, 17869.
- [39] H. Li, S. Liu, S. Yao, X. Wu, X. Hu, Y. Chen, *Energy Environ. Sci.* **2023**, *16*, 76.
- [40] J. Song, Y. Li, Y. Cai, R. Zhang, S. Wang, J. Xin, L. Han, D. Wei, W. Ma, F. Gao, Y. Sun, *Matter* **2022**, *5*, 4047.
- [41] H. Li, S. Liu, X. Wu, Q. Qi, H. Zhang, X. Meng, X. Hu, L. Ye, Y. Chen, *Energy Environ. Sci.* **2022**, *15*, 2130.
- [42] D. Wang, G. Zhou, Y. Li, K. Yan, L. Zhan, H. Zhu, X. Lu, H. Chen, C. Z. Li, *Adv. Funct. Mater.* **2021**, *32*, 2107827.
- [43] H. Xia, Y. Zhang, W. Deng, K. Liu, X. Xia, C. J. Su, U. S. Jeng, M. Zhang, J. Huang, J. Huang, C. Yan, W. Y. Wong, X. Lu, W. Zhu, G. Li, *Adv. Mater.* **2022**, *34*, e2107659.
- [44] B. Fan, F. Lin, J. Oh, H. Fu, W. Gao, Q. Fan, Z. Zhu, W. J. Li, N. Li, L. Ying, F. Huang, C. Yang, A. K. Y. Jen, *Adv. Energy Mater.* **2021**, *11*, 2101768.

- [45] D. Wang, H. Liu, Y. Li, G. Zhou, L. Zhan, H. Zhu, X. Lu, H. Chen, C.-Z. Li, *Joule* **2021**, *5*, 945.
- [46] B. Fan, W. Gao, X. Wu, X. Xia, Y. Wu, F. R. Lin, Q. Fan, X. Lu, W. J. Li, W. Ma, A. K. Jen, *Nat. Commun.* **2022**, *13*, 5946.
- [47] H. Chen, H. Liang, Z. Guo, Y. Zhu, Z. Zhang, Z. Li, X. Cao, H. Wang, W. Feng, Y. Zou, L. Meng, X. Xu, B. Kan, C. Li, Z. Yao, X. Wan, Z. Ma, Y. Chen, *Angew. Chem., Int. Ed.* **2022**, *61*, e202209580.
- [48] Y. Zou, H. Chen, X. Bi, X. Xu, H. Wang, M. Lin, Z. Ma, M. Zhang, C. Li, X. Wan, G. Long, Y. Zhaoyang, Y. Chen, *Energy Environ Sci.* **2022**, *15*, 3519.
- [49] W. R. Mateker, M. D. McGehee, *Adv. Mater.* **2017**, *29*, 1603940.
- [50] E. Ravishankar, R. E. Booth, C. Saravitz, H. Sederoff, H. W. Ade, B. T. O'Connor, *Joule* **2020**, *4*, 490.